IUPAC Task Group on Atmospheric Chemical Kinetic Data Evaluation
Data Sheet V.A2.13 MD13

The citation for this datasheet is: Crowley, J. N., Ammann, M., Cox, R. A., Hynes, R. G., Jenkin, M. E., Mellouki, A., Rossi, M. J., Troe, J., and Wallington, T. J., Atmos. Chem. Phys., 10, 9059-9223, 2010; IUPAC Task Group on Atmospheric Chemical Kinetic Data Evaluation, http://iupac.pole-ether.fr.
This data sheet last evaluated: June 2017; last change in preferred values: June 2017

H_2O_2 + mineral oxide (dust) surfaces

Experimental data

Parameter	Substrate	p_{H2O2} /mbar	Temp./K	RH /%	Reference	Technique/ Comments
Uptake coefficients: γ						
1.5×10^{-3}	TiO_2	1.7×10^{-4}	295	15	Pradhan et al., 2010a	AFT-CIMS (a)
5.0×10^{-4}	TiO_2			70		
$(3.33 \pm 0.26) \times 10^{-4}$	Gobi sand	1.7×10^{-4}	295	15	Pradhan et al., 2010b	AFT-CIMS (b)
$(6.03 \pm 0.42) \times 10^{-4}$	Gobi sand			70		
$(6.20 \pm 0.22) \times 10^{-4}$	Saharan dust			15		
$(9.42 \pm 0.41) \times 10^{-4}$	Saharan dust			70		
$(1.21 \pm 0.04) \times 10^{-7}$	α-Al_2O_3	1.3×10^{-3}-1.4×10^{-2}	295	2	Zhao et al., 2011	Grid-FTIR (c)
$(0.76 \pm 0.09) \times 10^{-8}$				76		
$(1.55 \pm 0.14) \times 10^{-8}$	SiO_2	1.3×10^{-3}-1.4×10^{-2}	295	2		
$(0.61 \pm 0.06) \times 10^{-8}$				76		
$\gamma_{0,BET}=(1.0 \pm 0.1) \times 10^{-4}$	α-Al_2O_3	4.1×10^{-6}-9.9×10^{-5}	298		Wang et al., 2011	Kn-MS (d)
$\gamma_{ss,BET}=1.1\times10^{-5}$						
$\gamma_{0,BET}=(1.7 \pm 0.2) \times 10^{-4}$	MgO	4.1×10^{-6}-9.9×10^{-5}	298			
$\gamma_{ss,BET}=1.6\times10^{-5}$						
$\gamma_{0,BET}=(9.7 \pm 2.0) \times 10^{-5}$	Fe_2O_3	4.1×10^{-6}-9.9×10^{-5}	298			
$\gamma_{ss,BET}=5.5\times10^{-5}$						
$\gamma_{0,BET}=(5.2 \pm 0.9) \times 10^{-5}$	SiO_2	4.1×10^{-6}-9.9×10^{-5}	298			
$\gamma_{0,BET}=(3.9 \pm 1.2) \times 10^{-3}$	TiO_2	9.9×10^{-5}	275	0.003	Romanias et al., 2012	CWFT-MS (e)
$\gamma_{0,BET}=(1.1 \pm 0.3) \times 10^{-3}$				6		
$\gamma_{0,BET}=(5.0 \pm 1.5) \times 10^{-4}$				25		
$\gamma_{0,BET}=(2.5 \pm 0.7) \times 10^{-4}$				83		
$\gamma_{0,BET,UV}=(9.6 \pm 2.7) \times 10^{-3}$		5.9×10^{-6}				
$\gamma_{0,BET,UV}=(2.0 \pm 0.7) \times 10^{-4}$		4.7×10^{-4}				
$\gamma_{ss,BET,UV}=(7.7 \pm 1.9) \times 10^{-3}$		5.9×10^{-6}				
$\gamma_{ss,BET,UV}=(2.9 \pm 0.7) \times 10^{-5}$		4.7×10^{-4}				
$\gamma_{ss,BET,UV}=(3.5 \pm 0.9) \times 10^{-3}$		1.9×10^{-5}		0.003-52		

$\gamma_{0,BET}=(7.1 \pm 1.4) \times 10^{-4}$ $\gamma_{0,BET}=(3.7 \pm 0.7) \times 10^{-4}$ $\gamma_{0,BET}=(3.0 \pm 0.6) \times 10^{-4}$ $\gamma_{0,BET}=(12.6 \pm 2.5) \times 10^{-5}$ $\gamma_{0,BET}=(6.9 \pm 1.4) \times 10^{-5}$ $\gamma_{0,BET}=(6.0 \pm 1.2) \times 10^{-5}$	$CaCO_3$ SiO_2	1.5×10^{-5}- 1.5×10^{-4}	253 298 313 253 298 313	0	Zhou et al., 2012	Kn-MS (f)
$\gamma_{0,BET}=(8.6 \pm 2.6) \times 10^{-4}$ $\gamma_{0,BET}=(2.4 \pm 0.7) \times 10^{-4}$ $\gamma_{0,BET}=1.1\times 10^{-3}/(1+RH^{0.93})$ $\gamma_{ss,BET}=(8.5 \pm 2.5) \times 10^{-5}$ $\gamma_{ss,BET}=(1.0 \pm 0.3) \times 10^{-6}$ $\gamma_{0,BET,UV}=8.7 \times 10^{-4}/(1+5.0\times 10^{13}exp(-9700/T))$ $\gamma_{0,BET}=(9.0 \pm 2.7) \times 10^{-4}$ $\gamma_{0,BET}=(3.7 \pm 1.1) \times 10^{-4}$ $\gamma_{0,BET}=1.1 \times 10^{-3}/(1+RH^{0.73})$ $\gamma_{0,BET,UV}=9.3 \times 10^{-4}/(1+3.6\times 10^{14}exp(-10300/T))$	α-Al_2O_3 Fe_2O_3	6.3×10^{-6} 7.0×10^{-4} 1.9×10^{-5} 6.3×10^{-6} 7.0×10^{-4} 1.9×10^{-5} 6.0×10^{-6} 6.5×10^{-4} 1.9×10^{-5} 1.9×10^{-5}	300 268-320 300 268-320	0.005 0-80 0.005 0.3 0.005 0-80 0.3	Romanias et al., 2013	CWFT-MS (g)
$\gamma_{ss,BET}=(6.5 \pm 0.6) \times 10^{-7}$ $\gamma_{ss,BET}=(8.6 \pm 0.8) \times 10^{-8}$	$CaCO_3$	5.4×10^{-3}	298	3 75	Zhao et al., 2013	Grid-FTIR (h)
$\gamma_{0,BET}=(4.2 \pm 1.3) \times 10^{-4}$ $\gamma_{0,BET}=(3.0 \pm 1.0) \times 10^{-4}$ $\gamma_{0,BET,UV}=3.2 \times 10^{-4}/(1+2.5\times 10^{10}exp(-7360/T))$ $\gamma_{ss,BET}=(1.1 \pm 0.3) \times 10^{-4}$ $\gamma_{ss,BET}=(1.4 \pm 0.4) \times 10^{-5}$ $\gamma_{0,BET}=4.8 \times 10^{-4}/(1+RH^{0.66})$ $\gamma_{ss,BET}=(1.0 \pm 0.3) \times 10^{-5}$ $\gamma_{ss,BET,UV}=(2.1 \pm 0.6) \times 10^{-5}$	ATD	7.4×10^{-6} 2.1×10^{-4} 4.1×10^{-5} 7.4×10^{-6} 2.1×10^{-4} 3.8×10^{-5} 3.8×10^{-5} 4.1×10^{-5}	300 268-320 300 300 275 275 268-320	0 0.3 0-69 2-69 0.3	El Zein et al., 2014	CWFT-MS (i)
$\gamma_{ss}=1.0\times10^{-4}/(1-0.042\times RH^{0.59})$ $\gamma_{ss}=3.3\times10^{-4}/(1+0.019\times RH^{1.1})$	ADS ATD	5.2×10^{-7}	298	3-90	Wu et al., 2015	Filter-HPLC (j)
$\gamma_{0,BET}=(1.5 \pm 0.3) \times 10^{-4}$ $\gamma_{0,BET}=exp(931/T-11.9)/(1+exp(931/T-11.9))$ $\gamma_{ss,BET}=(1.0 \pm 0.2) \times 10^{-4}$ $\gamma_{0,BET}=(2.4 \pm 0.5) \times 10^{-4}$ $\gamma_{0,BET}=exp(644/T-10.5)/(1+exp(644/T-10.5))$ $\gamma_{ss,BET}=(1.1 \pm 0.2) \times 10^{-4}$ $\gamma_{0,BET}=(5.3 \pm 1.3) \times 10^{-5}$ $\gamma_{0,BET}=exp(941/T-13.0)/(1+exp(941/T-13.0))$ $\gamma_{ss,BET}=(4.2 \pm 0.9) \times 10^{-5}$	ATD Mong. D. Xingj. D.	1.5×10^{-5} 1.5×10^{-5} 1.5×10^{-5}	298 253-313 298 298 253-313 298 298 253-313 298	0 0 0	Zhou et al., 2016	Kn-MS (k)

desorption rate coefficient, k_d, / s^{-1}					
$(5.6 \pm 0.7) \times 10^{-4}$	$CaCO_3$	1.5×10^{-5}-	253	Zhou et al., 2012	Kn-MS (f)
$(8.9 \pm 1.2) \times 10^{-4}$		1.5×10^{-4}	283		
$(2.6 \pm 0.1) \times 10^{-4}$	SiO_2	1.5×10^{-5}-	253		
$(4.6 \pm 0.2) \times 10^{-4}$		1.5×10^{-4}	313		

Comments

(a) H_2O_2 (initial concentration ≈ 4.1×10^{12} molecule cm^{-3}) was detected by CIMS using CF_3O^- as a reagent ion. A sub-micron aerosol was generated by nebulising an aqueous dispersion of TiO_2 particles. Particle number and size distribution was analysed using a DMA, D_{max} was 0.45 μm at 40% RH.

(b) Experimental method as in comment (a). For Gobi sand the available surface area was mainly from particles of diameter ~0.4 μm, for Saharan dust ~0.2 μm.

(c) SiO_2 (5.5 mg, (440±12) m^2 g^{-1}) and α-Al_2O_3 (15.5 mg, (32.8±1.6) m^2 g^{-1}) were pressed onto a stainless steel mesh, which was inserted into a cylindrical FTIR reactor. H_2O_2 was monitored by HPLC. Uptake coefficients were derived from the time dependent increase of absorbance at 2828 cm^{-1} (SiO_2) and 2805 cm^{-1} (α-Al_2O_3), using the BET specific surface area. The resulting γ_{BET} were independent of sample mass. Substrate bound H_2O_2 accounted for approximately 53% (SiO_2) and 29% (α-Al_2O_3) of the H_2O_2 loss from the gas phase. H_2O_2 turnover exceeded monolayer equivalent based on BET area after long exposure times, indicating catalytic loss.

(d) Knudsen reactor operated at 1.4×10^{-8} mbar. α-Al_2O_3 (1 μm particle diameter, 9.24 m^2 g^{-1}), MgO (1 μm particle diameter, 7.33 m^2 g^{-1}), Fe_2O_3 (0.7 μm particle diameter, 5.59 m^2 g^{-1}) and SiO_2 (0.5 μm particle diameter, 7.21 m^2 g^{-1}) samples applied as aqueous slurries followed by drying in vacuum. H_2O_2 was admitted by a leak valve and detected at m/z = 34. Uptake coefficients in the linear mass dependent range were used to derive γ_{BET}. Integrated uptakes exceeded monolayer equivalents (on a BET basis), indicating catalytic behaviour. O_2 was observed as product from H_2O_2 interacting with Fe_2O_3.

(e) TiO_2 films of Aeroxide P25 (50 ± 15 m^2 g^{-1} surface area, ~20 nm particle diameter) were cast on the outer surface of a Pyrex tube (0.9 cm outer diameter) as a suspension in ethanol, followed by drying and baking at 100-150°C in vacuo. For UV irradiation experiments, fluorescent lamps (315-400) nm, were used. leading to J_{NO2} in the range (0.002-0.012) s^{-1}. H_2O_2 was measured at m/z = 34. The pressure dependence of the first order loss rate was used to obtain the gas phase diffusion coefficient of H_2O_2 in He of D_0 = 415±35 Torr cm^2 s^{-1}. This value was used in deriving the geometric uptake coefficient. The uptake coefficients are based on BET surface area, γ_{BET}, and were obtained from γ in the linear mass dependent regime. $\gamma_{0,BET,UV}$ or $\gamma_{ss,BET,UV}$ reported in the table refer to irradiation with J_{NO2} = 0.012 s^{-1}. Conversion of added NO to NO_2 indicated the formation of HO_2 as a product of the photo-decomposition of H_2O_2. The HO_2 yield could not be quantitatively assessed due to secondary loss of HO_2 and other oxidation processes of NO on TiO_2.

(f) Same Knudsen reactor setup and detection as in (d), SiO_2 (2 μm particle diameter, 6.42 m^2 g^{-1}) and $CaCO_3$ (5 μm particle diameter, 1.07 m^2 g^{-1}) samples applied as aqueous slurries followed by drying in vacuum. Uptake was interpreted as reversible adsorption; the adsorption enthalpy derived from plots of the temperature dependence of $\gamma_{BET}/(1- \gamma_{BET})$ was –(7.8 ±1.6) kJ mol^{-1} and –(9.9 ±2.0) kJ mol^{-1} for SiO_2 and $CaCO_3$, respectively, while the activation energy of desorption obtained from the temperature dependence of the desorption rate coefficient, k_d, was (9.2 ±0.1) kJ mol^{-1} and (5.9 ±0.9) kJ mol^{-1}, respectively.

(g) Same experimental set up as (e); γ-Al_2O_3 and Fe_2O_3 had specific surface areas of (200±20) m^2 g^{-1} and (11±2) m^2 g^{-1}, respectively. Uptake was mostly irreversible and clearly exceeded

monolayer equivalents. UV irradiation had no effect on either the initial or steady state uptake coefficients. The temperature dependence experiments were performed at constant relative humidity and thus at variable absolute partial pressure of H_2O vapour, casting some uncertainty on the kinetic interpretation of the temperature dependence of the uptake coefficient.

(h) Same experimental technique as in (c); study mostly dedicated to experiments with $CaCO_3$ samples processed with HNO_3 and SO_2. Only results with pure $CaCO_3$ are reported in the table. In addition, the authors did not provide absolute uptake coefficients due to uncertainties of the exposed surface area. For the sake of comparison, the uptake coefficients reported in the table have been calculated from the uptake rates reported by the authors in their Fig. 3a.

(i) Same experimental set up as (e); ATD (0-3μm) had a specific surface area of (85±10) $m^2\ g^{-1}$. Uptake was irreversible both under dark and UV conditions. The steady state uptake coefficient depended linearly on the UV irradiation intensity. Temperature dependence experiments were performed at constant relative humidity and thus at variable absolute partial pressure of H_2O vapour, casting some uncertainty on the kinetic interpretation of the temperature dependence of the uptake coefficient.

(j) Asian dust storm samples (ADS, 6.1 $m^2\ g^{-1}$) refer to airborne dust collected following a sand storm in Beijing, China. ATD (16.5 $m^2\ g^{-1}$) was obtained from the A1 ultrafine fraction of ATD. Both samples were re-suspended and deposited on a filter. H_2O_2 (510±40 pptv) was detected by HPLC. Uptake coefficients were calculated from the fractional loss of H_2O_2 across the filter. Since the study also involved ambient particles with unknown BET surface area, the effective surface areas were determined indirectly from the full sample mass dependence of the fractional H_2O_2 loss.

(k) Same experimental set up as (d), ATD (0-5 μm particle diameter, 5.3 $m^2\ g^{-1}$), Inner Mongolia desert dust (Mong, 5.1 $m^2\ g^{-1}$) and Xinjiang sierozem (Xingj, 21.0 $m^2\ g^{-1}$) samples applied as aqueous slurries followed by drying in vacuum. Uptake coefficients in the linear mass dependent range were used to derive γ_{BET}. While steady state uptake was observed, the initial uptake was interpreted as driven by mostly reversible adsorption; the adsorption enthalpy derived from plots of the temperature dependence of $\gamma_{0,BET}/(1-\gamma_{0,BET})$ was –(7.7 ±1.5) kJ mol^{-1} ,–(5.4 ±1.1) kJ mol^{-1} , and ,–(7.8 ±1.6) kJ mol^{-1} for ATD, Mong and Xinj, respectively. The activation energy for the surface reaction was obtained from the temperature dependence of $\gamma_{0,BET}/(1-\gamma_{0,BET})$ to be 8.64 kJ mol^{-1} and 18.4 kJ mol^{-1}, for ATD and Mong, respectively.

Preferred Values

Parameter	Value	T/K
γ (1-60 % RH)	10^{-4}	268-320
Reliability		
$\Delta \log(\gamma)$	±0.7	268-320

Comments on Preferred Values

Uptake of H_2O_2 on mineral dust under atmospheric conditions is a complex process, with substantially different pathways under dry and humid conditions. Given the differences in substrate material, experimental techniques, and time scales involved in the determination of γ_0, there is fair agreement among the different studies with respect to γ_0 values obtained under dry conditions (Figure 1, left panels). Most of the studies report uptake being irreversible also on short time scales, so that γ_0 values do likely not represent the accommodation coefficient, α_s, in spite of the

negative temperature dependence of γ_0 and also in spite of the insensitivity to the partial pressure of H_2O_2. γ_0 values more likely represent initial decomposition of H_2O_2 on the surface. Due to the similarly short time scale covered, the aerosol flow tube studies by Pradhan et al. (2010a, 2010b) are also included in the left panels of Figure 1 for comparison.

Steady state uptake coefficients, γ_{ss}, which reflect the more relevant long term loss of H_2O_2 in the atmosphere, exhibit markedly different behaviour as a function of H_2O_2 partial pressure, relative humidity and temperature, and also substantial scatter among the studies (right panels in Figure 1). The negative pressure dependence is due to depletion of reactive capacity and rather not due to adsorption saturation. We therefore prefer the studies performed at low H_2O_2 pressures and with authentic dust materials. Given that the aerosol flow tube studies by Pradhan et al. cover short time scales only, while otherwise best representing the physical characteristics of airborne particles, and given that the other studies rather underestimate uptake coefficients due to uncertainties in exposed surface area, the preferred value for γ is a reasonable representation of the available data. On pure proxy materials, uptake shows negative humidity dependence, indicating that competitive adsorption plays a role. The authentic materials do not show this trend; at high relative humidity, the uptake coefficient rather tends to increase for some of them, indicative of the transition into aqueous phase chemistry in adsorbed water or brine layers. This is reflected in a humidity independent recommendation limited to < 60 % RH. With respect to the temperature dependence, the available data show a slightly positive trend. This is, however, not considered significant, in view of the uncertainties related to the convolution of pressure, humidity and diffusion effects in the different experiments. This leads to a temperature independent recommendation with expanded error limits.

Mineral dust contains photocatalytically active transition metal oxides. As demonstrated for the case of pure TiO_2 by Romanias et al. (2012), this may lead to substantially increased H_2O_2 decomposition und UV light in the range of 300 to 400 nm (Figure 2). For other oxides, such as Al_2O_3 and Fe_2O_3, the effects are less pronounced. There are insufficient data on authentic mineral dust to provide a quantitative estimate of the effect of UV irradiation, and we recommend that a factor of two increase in γ should be considered in sensitivity studies. Yi et al. (2012) provide evidence for HO_2 production from the photochemical reaction of H_2O_2 with TiO_2; from the addition of various electron and hole scavengers, they conclude that HO_2 results from the reaction of H_2O_2 with OH or directly with holes.

References

Pradhan, M., Kalberer, M., Griffiths, P. T., Braban, C. F., Pope, F. D., Cox, R. A. and Lambert, R. M.: Environ. Sci. Technol., 44, 1360-1365, 2010a.

Pradhan, M., Kyriakou, G., Archibald, T., Papageorgiou, A. C., Kalberer, M., and Lambert, R. M.: Atmos. Chem. Phys. 10, 7127-7136, 2010b.

Romanias, M. N., El Zein, A., and Bedjanian, Y.: Atmos. Environ., 77, 1-8, 2013.

Romanias, M. N., El Zein, A., and Bedjanian, Y.: J. Phys. Chem. A, 116, 8191-8200, 2012.

Wang, W.-G., Ge, M.-f., and Sun, Q.: Ch. J. Chem. Phys., 24, 515-520, 2011.

Wu, Q. Q., Huang, L. B., Liang, H., Zhao, Y., Huang, D., and Chen, Z. M.: Atmos. Chem. Phys., 15, 6851-6866, 2015.

Yi, J., Bahrini, C., Schoemaecker, C., Fittschen, C., and Choi, W.: J. Phys. Chem. C, 116, 10090-10097, 2012.

Zein, A. E., Romanias, M. N., and Bedjanian, Y.: J. Phys. Chem. A, 118, 441-448, 2014.

Zhao, Y., Chen, Z., Shen, X., and Huang, D.: Atmos. Environ., 67, 63-72, 2013.

Zhao, Y., Chen, Z., Shen, X., and Zhang, X.: Environ. Sci. Technol., 45, 3317-3324, 2011.

Zhou, L., Wang, W., Ge, M., and Tong, S.: J. Environ. Sci., 40, 44-50, 2016.
Zhou, L., Wang, W.-G., and Ge, M.-F.: J. Phys. Chem. A, 116, 7959-7964, 2012.

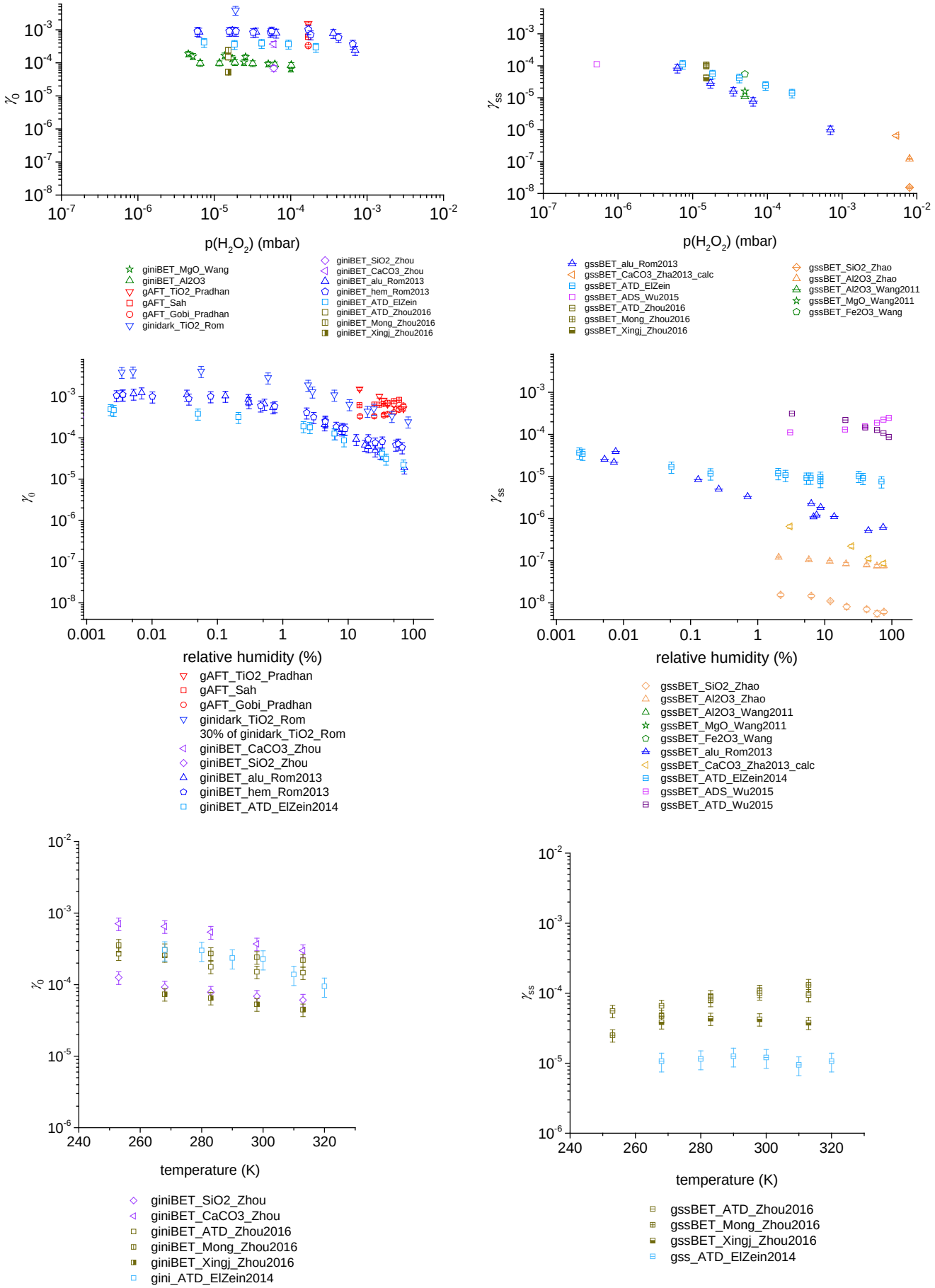

Figure 1: Initial (left) and steady state (right) uptake coefficient of H_2O_2 on mineral dust in the dark as a function of partial pressure of H_2O_2 (top), relative humidity (middle) and temperature (bottom); symbol shape codes the substrate type, symbol color codes the author / group.

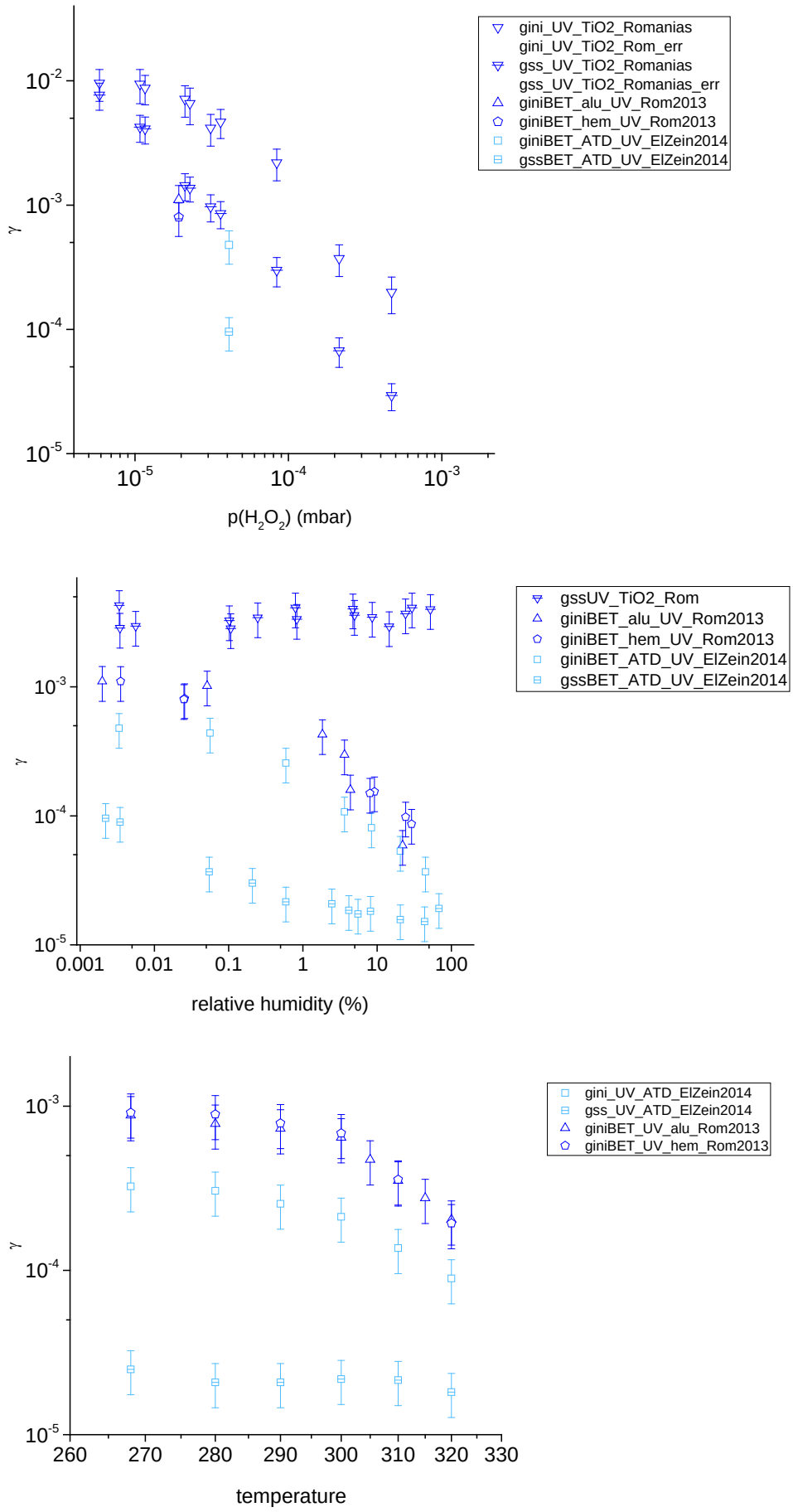

Figure 2: Uptake coefficient of H_2O_2 on mineral dust under UV (J_{NO2} = 0.012 s^{-1}) as a function of partial pressure of H_2O_2 (top), relative humidity (middle) and temperature (bottom). Colour and symbol shape code as in Figure 1.